Optics Letters

Convex silica microlens arrays via femtosecond laser writing

Jian-Guan Hua,[1] Hang Ren,[1] Ao Jia,[1] Zhen-Nan Tian,[1,5] Lei Wang,[1] Saulius Juodkazis,[3,4,6] Qi-Dai Chen,[1] and Hong-Bo Sun[1,2]

[1]State Key Laboratory of Integrated Optoelectronics, College of Electronic Science and Engineering, Jilin University, Changchun 130012, China
[2]State Key Laboratory of Precision Measurement Technology and Instruments, Department of Precision Instrument, Tsinghua University, Beijing 100084, China
[3]Centre for Micro-Photonics, Faculty of Science, Engineering and Technology, Swinburne University of Technology, Hawthorn, VIC 3122, Australia
[4]Melbourne Centre for Nanofabrication, ANFF, 151 Wellington Road, Clayton, VIC 3168, Australia
[5]e-mail: zhennan_tian@jlu.edu.cn
[6]e-mail: sjuodkazis@swin.edu.au

Received 24 September 2019; revised 9 December 2019; accepted 20 December 2019; posted 20 December 2019 (Doc. ID 378606); published 27 January 2020

We report fabrication of silica convex microlens arrays with controlled shape, size, and curvature by femtosecond laser direct writing. A backside etching in dye solution was utilized for laser machining high-fidelity control of material removal and real-time surface cleaning from ablation debris. Thermal annealing was applied to reduce surface roughness to 3 nm (rms). The good optical performance of the arrays was confirmed by focusing and imaging tests. Complex 3D micro-optical elements over a footprint of 100 × 100 μm^2 were ablated within 1 h (required for practical applications). A material removal speed of 120 μm^3/s (6 × 10^5 nm^3/pulse) was used, which is more than an order of magnitude higher compared to backside etching using a mask projection method. The method is applicable for fabrication of micro-optical components on transparent hard materials.

https://doi.org/10.1364/OL.378606

Nature's reply to light weight and fast imaging is a compound eye. The larger the number of lenslets, the faster the detection of direction and speed [1]. Microlens arrays (MLAs) have been used widely in optical imaging, beam shaping, and optical sensing [2,3]. They can improve integration, weight, and optical alignment by virtue of the small size and volume. However, there are challenges in fabrication of convex lens arrays on hard materials (in comparison with concave ones) especially due to the lack of lapping and polishing solutions for micro-sized objects. Current methods for fabricating MLAs include two-photon polymerization [4], lithography with masks [5], digital micro-mirror mask-less lithography [6], and thermal embossing [7]. These methods can be used to fabricate only polymer microlenses, which are difficult to use in harsh environments such as high temperature and high pressure. Diamond turning can machine hard materials, but its processing accuracy is not satisfactory at micro-scale. Dry or wet etching assisted femtosecond laser (fs-laser) machining can fabricate MLAs with good surface quality on glass, sapphire, and other materials [8] but the microlenses are concave, and it is difficult to control the size, curvature, surface shape, and other parameters of the lens for the required optical performance. The concave lens array has only a virtual focus, which greatly limits its applications.

As a high-precision, true three-dimensional (3D), cold-working technology, femtosecond laser direct writing (FsLDW) has been applied to preparation of micro-optical [9–13] and micro-mechanical [14,15] devices. 3D objects are usually prepared in photoresists based on laser polymerization [14,16]. However, the higher peak intensity of fs-laser pulses makes it possible to interact with any hard material in nature. By direct laser ablation, it is difficult to fabricate 3D structures with the high quality required for optical performance. The surface roughness is poor due to plasma formation and erosion during processing, and the debris condensation on the surface hinders 3D laser writing.

Fs-laser ablation requires high-energy intensity to achieve nonlinear absorption [17]. In this work, the FsLDW technology is used to process quartz glass in dye solution with low surface tension, as shown in Fig. 1(a), which can enhance the absorption of a UV laser to promote energy deposition near the silica surface [17] and produce stable bubbles to clean the debris generated during ablation in real time. Thus, 3D laser backside ablation can be performed. Convex MLAs on the silica surface were fabricated. The surface roughness of the lens was further improved by an annealing step, as shown in Figs. 1(b) and 1(c). Flexibility of the method allows for an easy control of arrangement of the lens array, size, curvature, and surface quality of the lens. Independent control of the focal length of each lenslet in the array is demonstrated and can be useful for focusing-free, fast imaging.

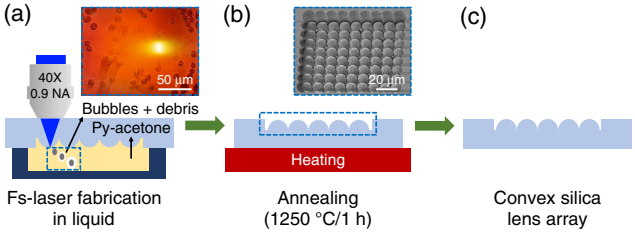

Fig. 1. Schematics of MLA fabrication. (a) Fs-laser fabrication in Py-acetone solution. Inset: bubbles dynamic image during ablation. (b) Annealing at 1250°C for 1 h. Inset shows the MLA before annealing. (c) MLA after annealing.

Fused silica (Jinlong photoelectric, Ltd., JGS1) was used for laser fabrication as received after washing in acetone. The dielectric strength of silica, ~500 MV/m, is more than two orders of magnitude higher than that in air, 3 MV/m. This allows to reach high intensity at the laser focus, even for the short wavelength used in this study, without dielectric breakdown of the host silica. This is an important advantage in backside etching as compared with front ablation with pre-surface air breakdown.

A laser (Pharos, Light Conversion Ltd.) operated at wavelength $\lambda = 343$ nm and pulse duration $t_p = 280$ fs was used for laser fabrication at a repetition rate of $f_l = 200$ kHz and linear beam scanning speed of $v_s = 10$ mm/s. The UV wavelength enables higher resolution of structuring compared to visible and infrared wavelengths, and the main advantage is a direct absorption (via a one-photon process) of dye pyrene (Py) solution to promote laser ablation of an irradiated backside surface. Polarization of the laser beam was set circular in order to reduce the effect of ripple formation on the ablated surfaces. Scanning was realized with a galvanometric mirror unit (Sunny Technology Ltd.) combined with linear stages (PI, P-611ZS) when translational replication over areas exceeding one write field were implemented. The distance between ablation layers along the direction of laser beam propagation was set at $\Delta z = 20$ nm, while the lateral shift within the layer in the xy plane was 50 nm between the adjacent raster lines. At $v_s = 10$ mm/s, $n = 9.3$ pulses were accumulated over the focal spot diameter d at the $f_l = 200$ kHz repetition rate.

The objective lens used for focusing had a numerical aperture of NA = 0.9 (S Fluor Nikon, $40^{\times}$ magnification). The objective was capable of compensating for the spherical aberration through a 0.11–0.23 mm thick cover glass and had a working distance of 0.3 mm. Transmission of the objective at 343 nm was measured directly and was $T = 60\%$. The pulse energy (fluence, irradiance) was calculated at the point of irradiation. The diameter of the focal spot was $1.22\lambda/\mathrm{NA} \approx 465$ nm.

The best performance in the backside ablation in Py–acetone 0.1 M solution pulse energy $E_p = 10$ nJ was required at $F_p = 5.6\ \mathrm{J/cm^2}$, $I_p = 19.6\ \mathrm{TW/cm^2}$. In these conditions, the pulse power was $E_p/t_p = 0.03$ MW/pulse, which is below the self-focusing threshold in silica, and a well-directed energy deposition at the silica–solution interface was made.

Annealing was carried out in an oven (Cinite, Ltd.) at temperature $T_a = 1250$°C, close to silica softening, for 1 h.

We used an acetone to dissolve the Py, which has the strongest absorption at 343 nm. The surface tension of acetone, $\gamma = 25.20$ mN/m, is smaller than that of water, 75.64 mN/m, which facilitates an effective surface wetting and debris removal from surfaces during ablation. Bubble formation and removal from the surface due to a pressure difference inside the bubble and surrounding pressure in the liquid, $\Delta P = 4\gamma/r_b$, will occur for the smaller radius r_b in acetone as compared with water. This was corroborated in experiment, when formation of large micro-bubbles was detrimental for maintaining a stationary surface ablation in water, while in acetone, smaller bubbles and their continuous departure from the silica–solvent interface helped a well-controlled machining of the surface. Formation of ablation ripples with a period of $\Lambda = \frac{\lambda_l}{2n} \approx 123$ nm was partially reduced by use of circular polarization; $n = 1.4$ is the refractive index of silica. The residual surface roughness after the laser ablation step was 100 nm (min-max) as determined by optical profilometry and atomic force microscopy (AFM). This roughness was reduced by high-temperature annealing at 1250°C for 1 h. The glass transition temperature of silica is 1180°C. Excessive annealing temperature and time will lead to a deviation in structure height. We found empirically that 1 h annealing at 1250°C was already smoothing the surface to the 3 nm (rms) roughness and could control the deviation of height within 2%. When annealing time was doubled, a rounding of the tips of the axicons occurred and flattening of the lens profile.

Large volumes of glass can be removed by ablation of the interface in direct contact with strongly absorbing dye solution. Different convex lenses were fabricated. The focal length for focusing in air is defined as $f = R/(n-1)$ for a spherical lens, where $n \approx 1.45$ is the refractive index of silica, and R is the curvature radius of the lens defined by the height h and diameter of the lens D as $R = \frac{h^2 + D^2/4}{2h}$. Scanning electron micrographs (SEMs) of a square convex spherical lens array are shown in Figs. 2(a) and 2(b). The lenses have very good surface quality and uniformity. The height of the lenses was characterized by confocal microscopy and showed a very good uniformity among the lenslets of the array. The curvature of the lenses was almost identical to the designed value: the diameter of a single lens was 12 μm, the radius of curvature was 8.5 μm (designed value 8 μm), and the focal length was $f = 19$ μm (designed value 18 μm). FsLDW can also be used to control the stacking mode of the lens at random. The photo-micrograph of the square-stacked MLA with a radius of curvature of 12.5 μm had a good surface topography [Figs. 2(e) and 2(f)]. Figures 2(g) and 2(h) show characterization of more closely packed hexagonal MLAs.

In order to verify optical performance of the MLA, it was tested by a 633 nm cw-laser. Figure 3(a) shows the focused light field of the lens array. The intensity and size of each focus is uniform for all lenslets of the array. The focal intensity distribution along a selected central section of the MLA [yellow frame in (a)] is shown in Fig. 3(b). In addition, a test of the imaging performance of the letter F [Fig. 3(c)] is shown in (d) and confirms uniform performance across all of the array as expected from the surface profile analysis (Fig. 2).

FsLDW has higher processing freedom as compared with other additive/subtractive manufacturing techniques and delivers high sub-wavelength resolution/precision of the surface finish. Also, it is easy to arbitrarily control the size of a single lens. As shown in Figs. 4(a) and 4(b), a very small diameter lens array can be made. The diameter of a single lenslet is only 5 μm and could be used as an optical element for a single CCD pixel. Such compound-eye lenses can be used in imaging systems without moving parts for fast frame capture. Patterns of $h = 3$ μm height would perform as antireflection surfaces for the wavelength of

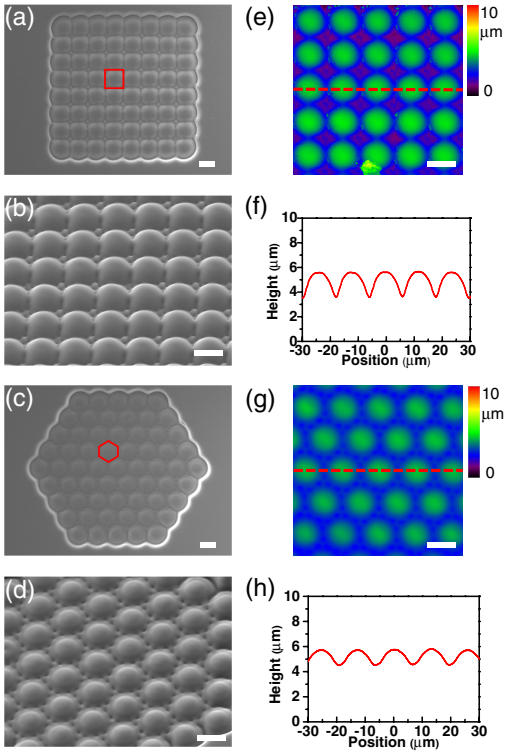

Fig. 2. SEM images of the square MLA: (a) top and (b) oblique views. SEM images of the hexagonal MLA: (c) top and (d) oblique views. (e), (f) Topography and altitude curve of the square MLA, respectively. (g), (h) Topography and altitude curve of the hexagonal MLA, respectively. Scale bars are 10 μm.

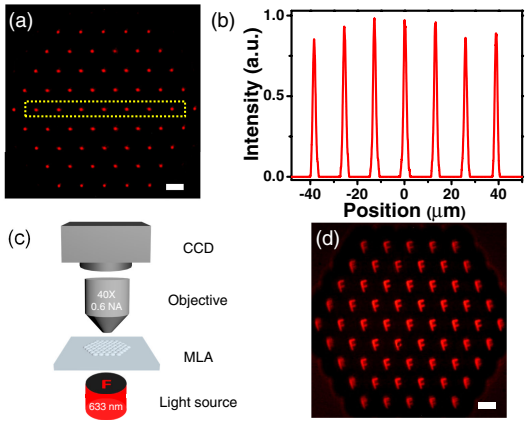

Fig. 3. Optical test for MLA. (a) Image of the focal plane. (b) Intensity cross sections of the region marked yellow in (a). (c) Schematic of the test setup. (d) Test image. Scale bars are 10 μm.

$\lambda_{AR} = 14.2$ μm at the spectral finger printing region and can be useful for micro-optical elements in miniaturized detection systems, $h_{AR} = \frac{\lambda_{AR}}{4\sqrt{n}}$ in air with $n = 1.4$ for silica. The curvature of a single lens can also be adjusted to follow the designed value. Figures 4(c) and 4(d) show a lens array having a larger curvature than that of the one in Fig. 2, with curvature radii of 7.5 μm and 11 μm, respectively. Figures 4(e) and 4(f) show a conical lens (axicon) array with a yellow curve presenting the

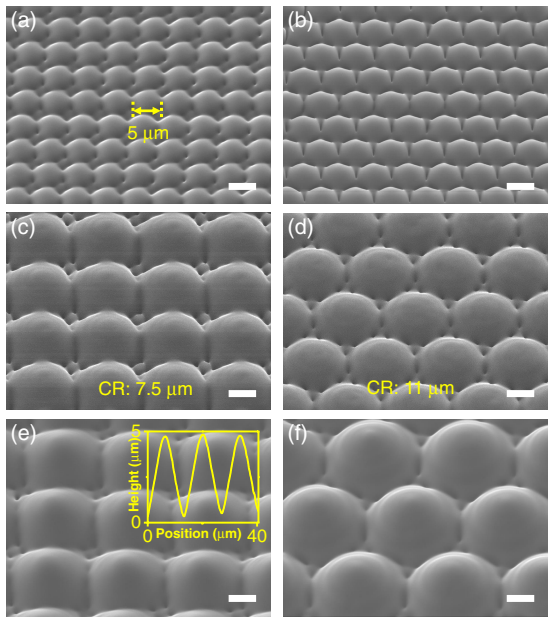

Fig. 4. SEM images of MLAs with different parameters. (a), (b) MLAs with small diameters; (c), (d) with large curvature radius (CR); (e), (f) conical axicon-type lenses. Scale bars are 5 μm.

height cross section of the lens. In sensor applications where imaging of moving objects is required, e.g., self-driving cars or security monitoring, robust micro-optical elements without moving parts should be used. For a MLA, this translates into imaging with different focal lengths at different segments of the MLA. This capability is readily met with the proposed laser sculpturing described above. Figure 5 shows a lens with lenslets having different focal lengths. The differences in curvature were $R = 10.6$ μm and 21.5 μm, which corresponded to a difference in focal length of $\Delta f = 24$ μm. The focal lengths of the three types of lenses shown in Fig. 5 are 24 μm, 33 μm, and 48 μm, respectively. Such types of MLAs can be integrated in microfluidics for monitoring of micro-objects at different depths. The strong stability, mechanical properties, and curved surface controllability of the silica lenses are the outstanding advantages compared with microlenses fabricated by other methods [4,8].

It is instructive to estimate the rate of material removal at the used conditions in this study. The typical ablation rate for MLA fabrication was $V_a/t_a = 9.93$ μm^3/s or 5×10^4 nm^3/pulse for intricate MLAs with small curvature radii, and was 120 μm^3/s for material removal in the case of a rectangular pit. The rate ~10 μm^3/s is higher by more than 10 times as compared with laser-induced backside wet etching (LIBWE) using mask projection lithography for silica in a Py–toluene solution [18]. The limiting factor in LIBWE is a required low repetition rate of tens of kHz due to bubble formation over the entire UV exposed area of the interface. In our study, tightly focused UV fs-laser pulses generated bubbles 3–5 μm in diameter, which swiftly departed from the surface and did not cause any disruption for ablation. Even higher repetition rates up to 600 kHz can be used and will be tested in the future.

Let us compare the efficiency of laser ablation in the backside etching mode with other methods. The fastest material removal for a dielectric was reported in a burst mode of dental tissue ablation using ultra-short ~800 fs laser pulses

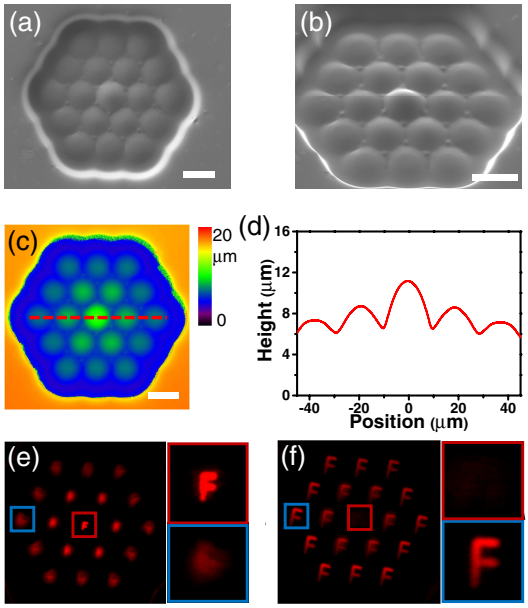

Fig. 5. SEM images of a compound microlens: (a) top and (b) oblique views. (c), (d) Topography and cross-sectional profile, respectively. (e), (f) Imaging test photographs: (e) center and (f) out-of-center show clear images. Scale bars are 20 μm.

[19] reaching $V_r = 5 \times 10^7\ \mu m^3/s$ with $N_{ib} = 25$ pulses (in a burst) of $E_p = 4\ \mu J$/puls e energy at $f_{ib} = 1.7$ GHz (in a burst) and separation between bursts at $f_{bb} = 1$ kHz rate. To access a measure of efficiency for ablation volume per single pulse at different processing regimes, we estimate removal rate per pulse and normalize it to energy as $\eta_p = V_r/(f_{bb} N_b E_p)[\mu m^3/\mu J/\text{pulse}]$; this estimate is still dependent on the in-a-burst frequency f_{ib}. The η_p increases for smaller E_p when f_{ib} is larger in a nonlinear way due to thermal accumulation [19]. For the burst removal of dental tissue, the efficiency per pulse was $\eta_p = 500\ \mu m^3/\mu J/\text{pulse}$. In our experiment of backside etching, we used 10^2-times smaller pulse energy, $E_p = 10$ nJ, as compared with burst ablation and $\eta_p = V_r/(f_{ib} E_p) = 5.1 \times 10^{-3}\ \mu m^3/\mu J/\text{pulse}$ for $f = 200$ kHz (in our non-burst case $f_{ib} = f$). The burst mode experiments showed that a high ~ GHz repetition rate facilitates energy deposition and absorption until the most efficient ablation per pulse is reached, while intra-burst time allows for required cooling in order to maintain the optimum. Too strong excitation results in the shallowest energy deposition into skin depth and reduces V_r and η_p. In our case of LIBWE, the energy was deposited at the interface considerably exceeding the ablation threshold of silica. The same argument of the ablation efficiency per energy deposition volume is important for optimization. We predict that a burst–LIBWE combination is a promising avenue to fast industrial throughput in 3D fabrication.

In conclusion, the backside ablation of silica by $E_p = 10$ nJ pulses at the interface with a strongly absorbing Py-acetone solution is shown to be a practical method (fabrication time ~ 1 h) for micro-optical elements over a footprint of $100 \times 100\ \mu m^2$. This method is applicable for removal of a large amount of silica (comparable with the volume of an optical element) validated by fabrication of MLAs. Fabrication throughput is comparable with that of 2D nanolithography writing tools: electron/ion beam lithography of hot-AFM-tip writers. There is essentially no material selectivity for laser ablation, and the method can be used for other materials.

Optical performance of fabricated structures was validated at 633 nm wavelength. By changing the radius of curvature of separate lenslets in the array, it is possible to achieve image formation without repositioning of the lens. This can find application in sensors and fast imaging applications. Lenses down to the size of an individual pixel in a CCD array can be fabricated with this method. In this study, we focused on a more demanding convex lens fabrication; however, this technique is also applicable to concave, free-form, aberration-corrected lenses, as well as flat diffractive optical elements where sharp phase steps have to be defined within a lateral length of ~ 1 μm.

Funding. National Basic Research Program of China (973 Program) (2017YFB1104600); National Natural Science Foundation of China (61825502, 61827826, 61590930, 61805100).

Acknowledgment. SJ is grateful for support via the ChangJiang Distinguished Professor project on 3D laser nano/micro-printing at Jilin University.

Disclosures. The authors declare no conflicts of interest.

REFERENCES

1. P. T. Gonzalez-Bellido, S. T. Fabian, and K. Nordström, Curr. Opin. Neurobiol. **41**, 122 (2016).
2. H. M. Kim, M. S. Kim, G. J. Lee, Y. J. Yoo, and Y. M. Song, Opt. Express **27**, 4435 (2019).
3. Z.-B. Fan, H.-Y. Qiu, H.-L. Zhang, X.-N. Pang, L.-D. Zhou, L. Liu, H. Ren, Q.-H. Wang, and J.-W. Dong, Light Sci. Appl. **8**, 67 (2019).
4. Z.-N. Tian, W.-G. Yao, J.-J. Xu, Y.-H. Yu, Q.-D. Chen, and H.-B. Sun, Opt. Lett. **40**, 4222 (2015).
5. W.-L. Liang, J.-G. Pan, and G.-D. J. Su, Optica **6**, 326 (2019).
6. B. Yang, J. Zhou, Q. Chen, L. Lei, and K. Wen, Opt. Express **26**, 28927 (2018).
7. Z. Deng, F. Chen, Q. Yang, H. Bian, G. Du, J. Yong, C. Shan, and X. Hou, Adv. Funct. Mater. **26**, 1995 (2016).
8. X.-Q. Liu, L. Yu, S.-N. Yang, Q.-D. Chen, L. Wang, S. Juodkazis, and H.-B. Sun, Laser Photon. Rev. **13**, 1800272 (2019).
9. J.-G. Hua, Z.-Y. Hu, S.-J. Xu, Z.-N. Tian, Y.-H. Yu, Q.-D. Chen, and H.-B. Sun, IEEE Photon. Technol. Lett. **31**, 3 (2019).
10. J.-G. Hua, Z.-N. Tian, S.-J. Xu, S. Lundgaard, and S. Juodkazis, Appl. Surf. Sci. **475**, 660 (2019).
11. M. Malinauskas, A. Zukauskas, S. Hasegawa, Y. Hayasaki, V. Mizeikis, R. Buividas, and S. Juodkazis, Light Sci. Appl. **5**, e16133 (2016).
12. L. Wang, Q.-D. Chen, X.-W. Cao, R. Buividas, X. Wang, S. Juodkazis, and H.-B. Sun, Light Sci. Appl. **6**, e17112 (2017).
13. L. Jiang, A.-D. Wang, B. Li, T.-H. Cui, and Y.-F. Lu, Light Sci. Appl. **7**, 17134 (2018).
14. H. Xia, J. Wang, Y. Tian, Q.-D. Chen, X.-B. Du, Y.-L. Zhang, Y. He, and H.-B. Sun, Adv. Mater. **22**, 3204 (2010).
15. K. Sugioka and Y. Cheng, Light Sci. Appl. **3**, e149 (2014).
16. J. Ni, C. Wang, C. Zhang, Y. Hu, L. Yang, Z. Lao, B. Xu, J. Li, D. Wu, and J. Chu, Light Sci. Appl. **6**, e17011 (2017).
17. R. Böhme, S. Pissadakis, D. Ruthe, and K. Zimmer, Appl. Phys. A **85**, 75 (2006).
18. Y. Kawaguchi, T. Sato, A. Narazaki, R. Kurosaki, and H. Niino, J. Photochem. Photobiol. A **182**, 319 (2006).
19. C. Kerse, H. Kalaycğlu, P. Elahi, B. Çetin, D. K. Kesim, Ö. Akçaalan, S. Yavaş, M. D. Aşık, B. Öktem, H. Hoogland, R. Holzwarth, and F. Ömer Ilday, Nature **537**, 84 (2016).